Construction and Building Materials 201 (2019) 1–10

Contents lists available at ScienceDirect

Construction and Building Materials

journal homepage: www.elsevier.com/locate/conbuildmat

Gypsum under tensile loading: A molecular dynamics study

Prodip Kumar Sarkar [a], Nilanjan Mitra [a,b,*]

[a] Department of Civil Engineering, IIT Kharagpur, Kharagpur 721302, India
[b] Centre for Theoretical Studies, IIT Kharagpur, Kharagpur 721302, India

HIGHLIGHTS

- Uniaxial and triaxial stress–strain response of single crystal gypsum under tension.
- Impact of different inter atomic energy components in the deformation response.
- Inter and intra layer separation is correlated to global stress–strain response.
- Layer slippage mechanism is investigated in conjunction with global response.

GRAPHICAL ABSTRACT

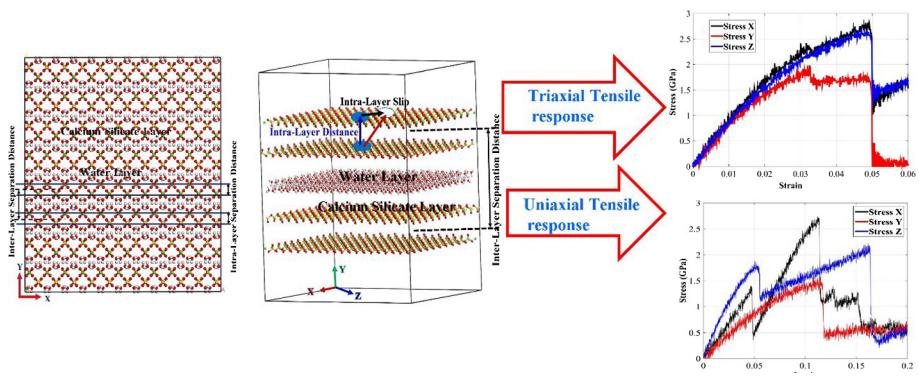

ARTICLE INFO

Article history:
Received 30 October 2018
Received in revised form 2 December 2018
Accepted 17 December 2018

Keywords:
Molecular dynamics
Uniaxial tension
Triaxial tension
Interlayer separation
Intralayer separation
Layer slippage

ABSTRACT

The behavior of pristine single crystal gypsum under tensile loading at a molecular level has been probed in this study based on simulations. Uniaxial stress type tensile loading situations demonstrate anisotropy in response. For both uniaxial and triaxial loading situations, the non-bonded part of the energy governs the response. The response behavior of the tensile stress strain curves in uniaxial and triaxial conditions have been correlated with changes in the molecular structure along with interlayer and intralayer separation distances and layer slippages.

© 2018 Elsevier Ltd. All rights reserved.

1. Introduction

Gypsum is a naturally available sulfate mineral, chemically known as hydrous calcium sulfate $CaSO_4 \cdot 2H_2O$. It is present as natural reserves in various parts of the world [1] and also in other planets such as Mars (as confirmed at ground level by Mars Exploration Rover Opportunity) [2]. The stability of the mineral on Mars was demonstrated in a recent study [3]. Gypsum was also observed to precipitate in natural sea ice [4]. It is one of the softest minerals with a Moh's hardness of 1.5–2.0. It can also exist in different forms based on the amount of the water retained between the layers of $CaSO_4$ structure such as in bassanite ($CaSO_4 \cdot H_2O$) and anhydrite ($CaSO_4$). It has been reported that understanding the behavioral mechanisms of hydrous phases of these naturally available minerals along with their phase transition characteristics under different loading situations is important in the study of Earth mantle dynamics which might reveal mechanisms for generation of deep focus earthquakes [5]. The hydration and dehydration cycles of

* Corresponding author at: Department of Civil Engineering, IIT Kharagpur, Kharagpur 721302, India.
E-mail address: nilanjan@civil.iitkgp.ernet.in (N. Mitra).

https://doi.org/10.1016/j.conbuildmat.2018.12.097
0950-0618/© 2018 Elsevier Ltd. All rights reserved.

these minerals also results in changes in the P and S wave velocities [6]. It has been reported in literature that under present environmental conditions polycrystalline gypsum first transforms to bassanite but ultimately dehydrates to anhydrite regardless of temperature [7]. There also exists studies in which pressure induced phase transition of gypsum has been carried out experimentally [8–10] in which the main focus of the study had been on characterization of different phases using Raman Spectroscopy and energy dispersive X-ray diffraction investigations. Theoretical studies also exist demonstrating the formation of higher pressure polymorphs of the material using density functional theory (DFT) [11]. The effect of Mg^{2+} impurity on the surface properties of Calcium sulfate hemihydrate has been investigated using DFT approach [12] which reveals a strong adsorption and substitution between the ion and the crystal plane $(2\,0\,0)_1$. MD simulation has been conducted to study the intrinsic morphology of $CaSO_4$ and its stable hydrates with the application of modified MSXX-F3C force field [13]. It has been concluded that the morphology of anhydrates, hemihydrate and fully hydrate of calcium sulfate are decahedral, rodlike and disk-like respectively.

Even though there has been numerous studies on the material, there does not exist studies which demonstrates the response mechanism of the material at a molecular level as it is mechanically loaded. Layered calcium sulfate materials share similarities with layered structures of calcium phosphates, calcium silicates and or calcium aluminates. The layered structure similarities as well as the water content in between the layers may explain the orientational anisotropy of these materials.

Mechanical loading of the material can happen due to many reasons such as hydration and dehydration cycle. These cycles can result in formation of pores and voids (due to dehydration of water) [14] or increase in pore pressure (due to water hydration) [7] which eventually leads to development of forces on the crystal structure leading to formation of cracks. It is well known from a mechanical perspective that cracks result due to tensile as well as shear loading of a material. Thereby, in this study only tensile loading has been considered.

Apart from naturally existing mineral deposits, gypsum is also mined and has numerous applications in different industries such as in infrastructure (gypsum boards, blocks, mortar, plaster as well as ingredients of Ordinary Portland cement in preventing flash set [15,16] and ingredients of calcium sulfoaluminate cements resulting in reactions with ye'elimite to form ettringite [17]), fertilizers and soil conditioner (binder in fast-dry tennis court clay), impression plasters in dentistry as well as in the field of arts (sculpture material). In all these applications of gypsum, it is quite probable that the material is subjected to tensile type loading situations which eventually might result in formation of cracks. Thereby there is a need to study the response behavior of the material subjected to tension at a crystal structure level.

With the above information in perspective for gypsum, this structure–property study of the material has been initiated to understand the changes in molecular structure of gypsum when it is subjected to tensile type of loading situations. Neutron diffraction studies revealed the molecular structure of gypsum [18] which has been considered in our study. Though it is understood that there may be presence of defects as well as other materials as impurities in naturally available gypsum, in this study we have considered pristine single crystals of gypsum to better understand the molecular mechanisms of the material subjected to tensile loads.

The choice of suitable force potential plays the most important role in any molecular dynamic simulation. Development of such potential particularly for gypsum has been demonstrated through the calculation of elastic constants and lattice parameters against the experimental values [19]. Even though the potential is effective in replicating the cell parameters, there are significant differences in the reported elastic constants with that of the experimental results [20]. For this particular study, INTERFACE force field [21] has been adopted as it can efficiently reproduce both the cell parameters as well as the elastic properties which are comparable to experimentally available reports. It would be noteworthy to mention a recent review article regarding the development of different force field and their application in cementitious material where INTERFACE force field has also been discussed along with several other force fields [22]. The author has also introduced a detailed review article on application of force field to simulate different organic, inorganic material and their interface [23] in comparison to the DFT approach.

Uniaxial tensile stress condition is implemented by the application of deformation in one direction and the directions perpendicular are left unrestricted and thereby the material can experience both changes in the volumetric and deviatoric response. This type of loading and boundary condition is quite typical for psedostatic loading conditions in an universal testing machine and/or in a split-hopkinson type experiments [24–26]. Triaxial tensile stress is implemented by applying the displacement along three mutually perpendicular directions in a way that they are in the ratio of their initial dimensions.

2. Simulation methodology

The neutron diffraction study [18] reveals that the atomic structure of gypsum is crystalline in nature and belongs to a space group $I2/a$. The unit cell is monoclinic in nature where c axis does not coincide with the morphological c axis (the axis indicates the direction of morphological elongation of gypsum crystal). The discrepancy has been addressed by a successful coordinate transformation to space group $A2/a$ [27] which has been adopted for this particular study. The lattice parameters for the reported unit cell are $a = 5.678$ Å, $b = 15.213$ Å, $c = 6.286$ Å and $\alpha = \gamma = 90^\circ$, $\beta = 114.08^\circ$. Gypsum is layered structure of SO_4^{2-} tetrahedra where two consecutive layers are attached by Ca^{2+} ions creating double sheet layers. The double sheet layers are separated with the presence of the water molecule trapped in between (Ref. Fig. 1a, b) are arranged perpendicular to Y directions.

Thermodynamically consistent INTERFACE force field has been used to model the interaction between different atoms in the simulation box [21]. The energy expression of PCFF force field [28] composed of quadratic bond, angle interaction and Coulombic and 9–6 Lennard-Jones (LJ) interactions (nonbonded) (ref Eq. (1)), has been adopted to fit the coefficients of INTERFACE force field which can effectively reproduce the experimentally measured parameters like cell parameters, surface/interface properties, mechanical properties and vibration spectra. In the energy expression, $K_0, r_0, K_\theta, \theta_0, \epsilon, \sigma$ represents the parametric coefficients for bond, bond angle and LJ interactions of atoms of the same types. The parameters in LJ expression, ϵ, and σ, for atom of different types under interaction are computed using sixth power combination rule. It is to be mentioned that atoms under bonded and angle interactions are excluded while calculating the nonbonded interactions.

$$E_{pot} = \sum_{\substack{ij \\ \text{bonded}}} K_{r,ij}(r_{ij} - r_{0,ij})^2 + \sum_{\substack{ijk \\ \text{bonded}}} K_{\theta,ijk}(\theta_{ijk} - \theta_{0,ijk})^2 + \frac{1}{4\pi\varepsilon_0} \sum_{\substack{ij \\ \text{nonbonded} \\ (1,3\ \text{excluded})}} \frac{q_i q_j}{r_{ij}} + \sum_{\substack{ij \\ \text{nonbonded} \\ (1,3\ \text{excluded})}} \varepsilon_{ij}\left[2\left(\frac{\sigma_{ij}}{r_{ij}}\right)^9 - 3\left(\frac{\sigma_{ij}}{r_{ij}}\right)^6\right] \quad (1)$$

Using molecular dynamics simulation, the elastic constants were estimated and validated against the available experimental/

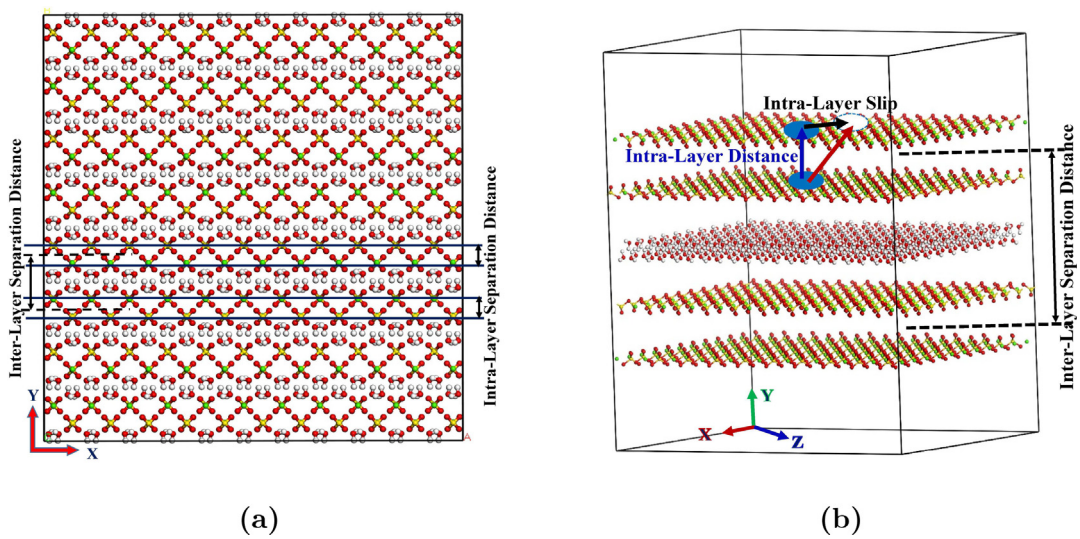

Fig. 1. The simulation box of gypsum consists of 11 × 4 × 10 supercells (Ca:green; S:Yellow; O:red; H:White) (a) projected at XY plane and (b) projected at XZ plane. (For interpretation of the references to colour in this figure legend, the reader is referred to the web version of this article.)

simulated results. This computation is performed in Material Studio [29] on a simulation box composed of 3 × 3 × 3 supercells with the help of INTERFACE force field. The energy minimization is performed on simulating system using smart minimization algorithm (combination of steepest descent, conjugate gradient and Newton–Raphson method) which ensure a stable configuration corresponding to the lowest energy state. The energy and force cut-off have been taken as 0.0001 kcl/mol, 0.005 kcl/mol/Å respectively. The dynamic calculation has been performed using the Newton's equation of motion with velocity-verlet time integration scheme (time step = 0.5 femtosecond) and randomly assigned initial velocities. The bulk system properties has been mimicked by Periodic Boundary Condition (PBC) which eliminates the disadvantage of boundary effect caused by the use of smaller simulation cell. The equilibration is performed under closed system (N), isobaric (P), isothermal (T) ensemble (NPT ensemble) for 200 ps which brings the configuration in equilibrium to room temperature (298 K) and atmospheric pressure (1 atm). Nose thermostat and Berendsen barostat has been selected in this thermodynamic equilibration process. For accurate calculation of non-bonded energy Ewald summation method is chosen with 6 Å repulsive cutoff and 0.0001 kcl/mol energy convergence limit.

Elastic constants has been evaluated with the help of constitutive relationship between stress tensor and strain tensor. The constitutive relationship (refer Eq. (2)) can be derived from 1st and 2nd law of thermodynamics assuming the elastic response as reversible process with zero dissipation. In static method, the entropic terms in the Helmholtz free energy (A) can be ignored and replaced by strain energy (U) (refer Eq. (2)) at moderate temperature isothermal process [30].

$$C_{ijkl} = \frac{1}{V_0}\frac{\partial^2 A}{\partial\varepsilon_{ij}\partial\varepsilon_{kl}}\bigg|_T = \frac{1}{V_0}\frac{\partial^2 U}{\partial\varepsilon_{ij}\partial\varepsilon_{kl}}\bigg|_T \tag{2}$$

In static approach a chosen numbers of strains below the elastic limit (±0.001 and ±0.003) have been used to deform the equilibrated configuration and subsequently energy minimization has performed on it to ensure the state of mechanical equilibrium. Numerical solution using Eq. (2) gives the elastic constants for a selected deformation level which are then averaged over all the other deformation levels. For this work ten such equilibrated configurations have been chosen and the ultimate constants are the average of all the constants computed for individual frames.

The evolution of the simulation system under uniaxial tension has been studied as the second part of this work where a larger simulation box composed of 11 × 4 × 10 supercells i.e. 62.458 × 60.852 × 62.86 Å^3 has been studied. Large Scale Massively Parallel Simulator (LAMMPS) [31] software package has been adopted for these simulations in which equilibration is performed on the energy minimized simulation box using isobaric-isothermal (NPT) ensemble with Nose thermostat and a Parrinello-Rahman barostat at ambient pressure (1 atm) and temperature (298 K) for 100 ps with a time step of 0.2 fs.

Uniaxial stress condition has been implemented by stretching the simulation box in the desired directions at a constant strain rate of 10^8 per second while the other two perpendicular directions are set to the zero target pressure using NPT ensemble which ensures no pressure variation in those directions. In order to implement a quasistatic type of loading situation, the simulation box has been relaxed under NVT ensemble upon each increment of strain value by 0.005 (similar strategy for studying uniaxial behavior using MD simulation has been done in literature [32–34]). The simulation has been carried on to attain a deformation up to a strain level of 0.2. Simulations have been carried out in X, Y and Z directions to check for anisotropy in the response.

Triaxial stress has been generated with the application of displacement along three mutually perpendicular directions with a constant strain rate of 10^8 per second and simultaneously the box has been relaxed under NVT ensemble at each 0.005 strain interval. The process is continued to 12 cycles which corresponds to the strain value of 0.06.

For both the deformation process, bulk nature of the system have been mimicked by periodic boundary condition (PBC). For the calculation non-bonded LJ interaction, a cut-off length of 12 Å is adopted for a faster simulation with reasonable accuracy level. Long-range electrostatics interactions has been captured through the use of particle–particle particle-mesh (PPPM) solver [35] with a convergence criterion of 10^{-6}.

3. Result and discussion

3.1. Elastic constants

As demonstrated from Table 1, the simulated equilibrated unit cell parameters for pristine single crystal gypsum closely matches

Table 1
Experimental and simulated unit cell parameters (simulation conditions: pressure = 1 atm and temperature = 298 K).

	a (Å)	b (Å)	c (Å)	α	β	γ
Simulated	5.726	15.342	6.339	90°	114.08°	90°
Experimental [20]	5.678	15.213	6.286	90°	114.08°	90°

that of experimental results (with variation between the simulated and experimental observations being less than 0.85%). The elastic constants as obtained from the simulation using the interface force potential also demonstrated good correlation to that of experimental results (ref Table 2). Infact our current simulated results are more closer to experimental observations compared to a previous published study using MD simulations [19]. This demonstrates that the force potential used in our study can be well utilized for observing response behavior of the material under different loading situations within reasonable accuracy.

3.2. Stress–strain relationship

The stress–strain response of gypsum subjected to uniaxial tensile loading (refer Fig. 2a) demonstrates an anisotropic nature of response. For the X and Z directions of loading, a drop in stress is observed at around 0.05 strain. However, the stress response increases after the drop. Similar type of drop in response is also observed for Y direction loading, albeit at different strain. Interestingly no such rise (as observed for X and Z directions) in stress–strain response after the initial drop is observed for the Y direction loading. The reason for this type of response may be due to the layered crystal structure of gypsum (note Y direction being perpendicular to that of the layers). The details for this has been probed in later sections. All drops are sharp which ensure the brittle nature of the material response. Energy decomposition plot in the X direction shows that the non-bonded part plays the main contributing role for the total energy (refer Fig. 2b). It can be observed that energy contribution due to bond stretch is negligible compared to the non-bonded energy as well as bond angle energy contribution. This suggests that instead of elongation of the bonds in the gypsum crystal, the angular changes as well as the van der Wall and Columbic interactions (parts contributing to the non-bonded energy component) plays a major role in the dynamics of the crystal structure subjected to the specified loading condition. It should also be noted that the energy due to bond angle starts contributing significantly only after strain level of 0.05 at which there is an expected change of the crystal lattice structure. Similar type of behavioral response for the energy contribution is observed for the Z direction (refer Fig. 3b). For the Y direction, it can be observed that the entire energy contribution is from the non-bonded energy (refer Fig. 3a). Comparing the maximum stress values it can also be observed that gypsum single crystal has differences in the load carrying capacity along the three orthogonal directions.

The triaxial stress–strain behavior (refer Fig. 4a) under tensile loading also demonstrates differences in response from 0.01 (around) strain and eventually a significant drop in response in the Y direction compared to that of the other two directions. The energy contribution is observed to be mainly governed by the non-bonded energies (refer Fig. 4b). This difference in behavior might be attributed to the differences in the crystal structure of the material since this layered material has layers along the X-Z plane and separated along the Y direction (refer Fig. 2b). Details of the differences between the responses has been explained later in the manuscript. Along the X and Z directions the stress–strain curve was observed to rise up but this has not been considered for this work since the response is unphysical as a clear

Table 2
Experimental and simulated elastic constants (simulation conditions: pressure = 1 atm and temperature = 298 K).

(×10 GPa)	C_{11}	C_{22}	C_{33}	C_{44}	C_{55}	C_{66}	C_{12}	C_{13}	C_{15}	C_{23}	C_{25}	C_{35}	C_{46}
Simulated	7.10	5.91	7.04	1.10	2.48	0.85	4.60	2.90	0.27	2.44	1.02	−1.40	0.27
Exp. [20]	7.86	6.27	7.26	0.91	2.64	1.04	4.10	2.69	−0.70	2.42	0.31	−1.74	−0.16
Ref. Study [19]	10.13	9.81	7.90	0.87	3.12	1.072	5.09	2.96	1.01	2.97	−0.74	2.60	0.12

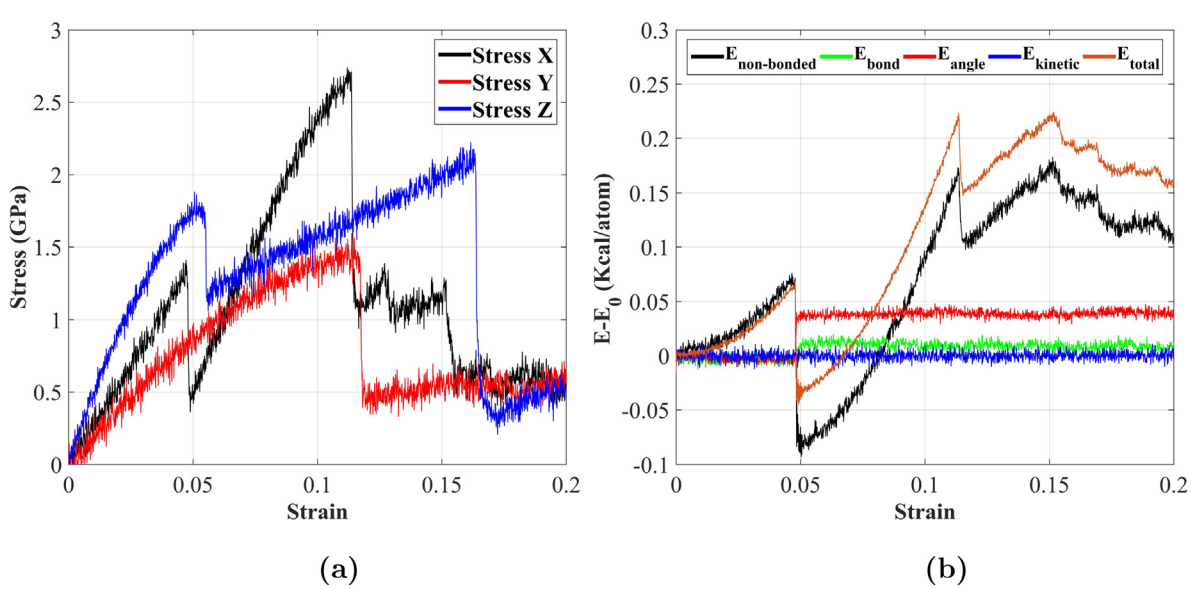

Fig. 2. (a) Uniaxial stress–strain behavior due to tensile deformation in X, Y and Z directions and (b) Energy decomposition of the simulating system under uniaxial deformation in X direction. (simulation conditions: pressure = 1 atm and temperature = 298 K).

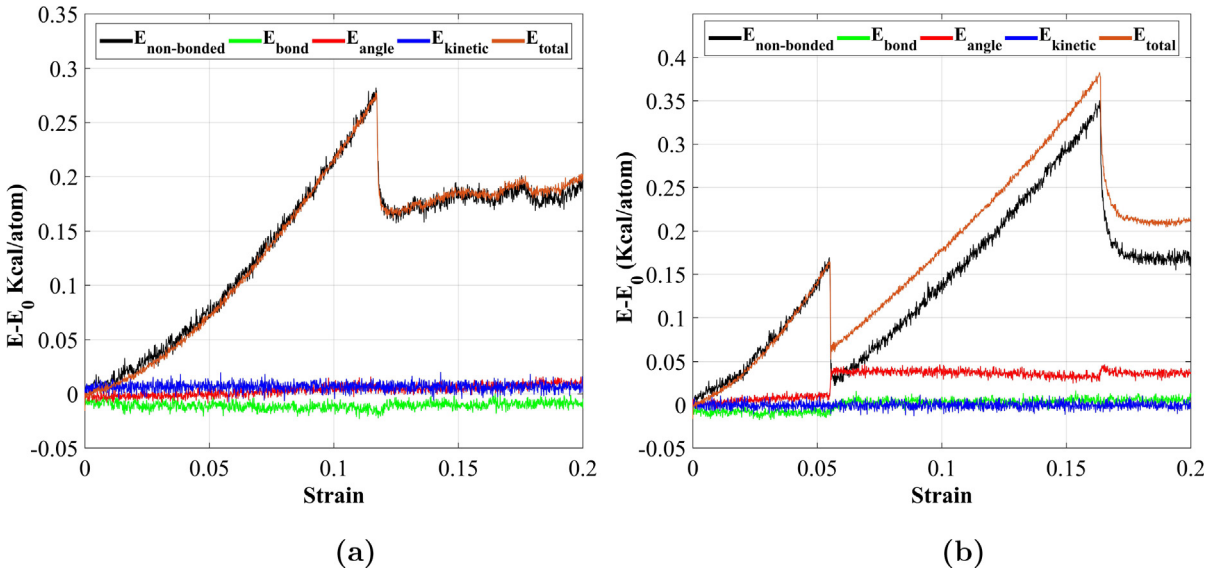

Fig. 3. (a) Energy decomposition of the system under uniaxial deformation in Y direction and (b) Energy decomposition of the system under uniaxial deformation in Z direction. (simulation conditions: pressure = 1 atm and temperature = 298 K).

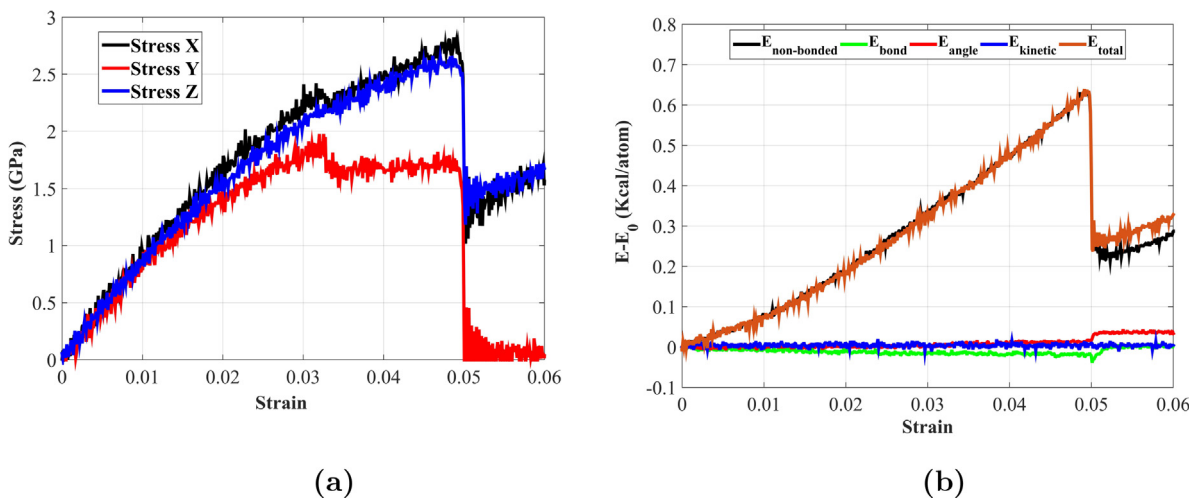

Fig. 4. (a) Stress–strain behavior under triaxial tensile deformation and (b) Energy decomposition of the system under triaxial tensile deformation. (simulation conditions: pressure = 1 atm and temperature = 298 K).

inter-layer separation is observed there after which has been discussed in details in later sections.

3.3. Layer separation study

Since the major energy contribution for loading along any directions for uniaxial loading as well as in the triaxial loading scenario is from the non-bonded parts, it is essential to understand the mechanism of change in the layered crystal structure which results in the non-bonded contribution.

The double sheet layers are separated with the presence of the water molecule trapped in between (Ref. Fig. 1a, b) being arranged perpendicular to Y directions.

Gypsum is composed of SO_4^{2-} double sheet layers attached in presence of Ca^{2+} ions and each double sheets are separated by a layer of water molecules (Ref. Fig. 1). For the demonstration purpose, the layers are classified as intra-layer and inter-layer. The inter-layer regions (typically having an average gap of around 7.5 Å) are separated by water molecules whereas the intra-layer regions (typically having an average gap of around 2.5 Å) are not. The layers in gypsum single crystal consists of SO_4^{2-} ions which are ionically bonded to that of the Ca^{2+} ions. Due to the presence of layered structure there is a possibility of the layers (both inter and intra) getting compressed or stretched as well as slip relative to each other; which has been probed in this study. This change in distance between the layers and/or slip between the layers mostly accounts for the non-bonded energy.

Fig. 5 shows evolution of layer distances against applied uniaxial tensile strain in three mutually perpendicular directions. It can be observed that for applied tensile strain in the Y direction, both the inter-layer as well as the intra-layer distances increase. On the other hand for tensile loading along the other two directions (along the two directions of the XZ plane on which layers are located) both the inter-layer as well as the intra-layer distances decrease due to Poissons' ratio effect. For the Y direction slightly above 0.1 strain, the inter-layer separation distance is observed

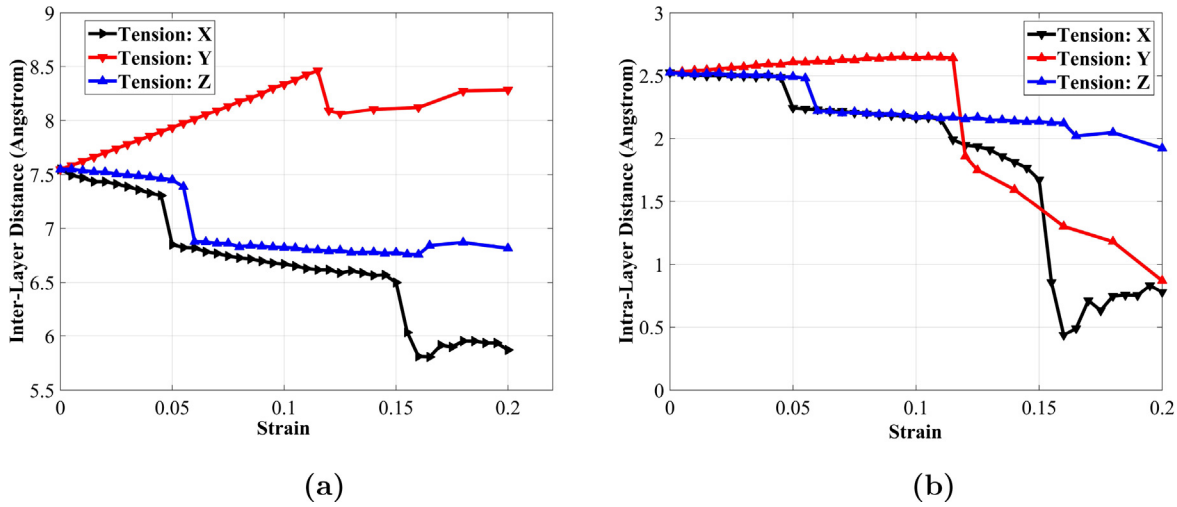

Fig. 5. (a) Evolution of Inter-layer distace for uniaxial tension and (b) Evolution Intra-layer distance uniaxial tension. (simulation conditions: pressure = 1 atm and temperature = 298 K).

to decrease which is also manifested by a drop in Y-direction stress–strain plot. Similar to observations in the X and Z direction stress–strain plots, inter-layer separation distance also undergoes a drop thereby demonstrating sudden closing of the two layers. Intra-layer separation distance for Y direction loading in the post-peak stress–strain regime shows that the distance between the two layers decreases more compared to the original separation distance (which is contrary to the behavior observed for Y direction inter-layer separation where the distance do not decrease more than the initial separation distance). X and Z direction intra-layer also demonstrates significant decrease in separation distance between the layers. The reason for the sharp increase or decrease in inter-layer and intra-layer response may be attributed to the changes in microstructural arrangement of the layers (which has been discussed in Layer Slippage Study subsection).

For the case of triaxial loading the stress–strain behavior along the X and Z directions are similar but there is a difference in behavior observed for the Y direction. No significant change is observed in the intra-layer and inter-layer distance for this type of loading condition in the pre-peak regime (refer Fig. 6a and b). In the post-peak regime a sharp drop is observed for the intra-layer distance which even goes below 0 indicating that there is an unphysical behavior, the reason of which is due to the sudden separation of two adjacent layers at strain level of 0.05 (refer Fig. 12). Interestingly it should be noted that no amorphization of the molecular structure is observed for this type of loading condition demonstrating significant differences of the observed response in uniaxial X and Z direction loading scenarios.

3.4. Layer slippage study

The evolution of layer slippage is shown in Fig. 7 which has been calculated from the relative change in the average gap between SO_4^{2-} groups in any two adjacent layers on XZ plane and then taking an average over all the other layers. So, the slip value is evaluated by deducing the current gaps of corresponding SO_4^{2-} groups from the value computed at initial stage (equilibrated sample). The ordinates represents the average relative slip between SO_4^{2-} sheets (including both the interlayer and interlayers) upon the increment of strain levels and the movement is being projected along mutually perpendicular X and Z directions as shown in the

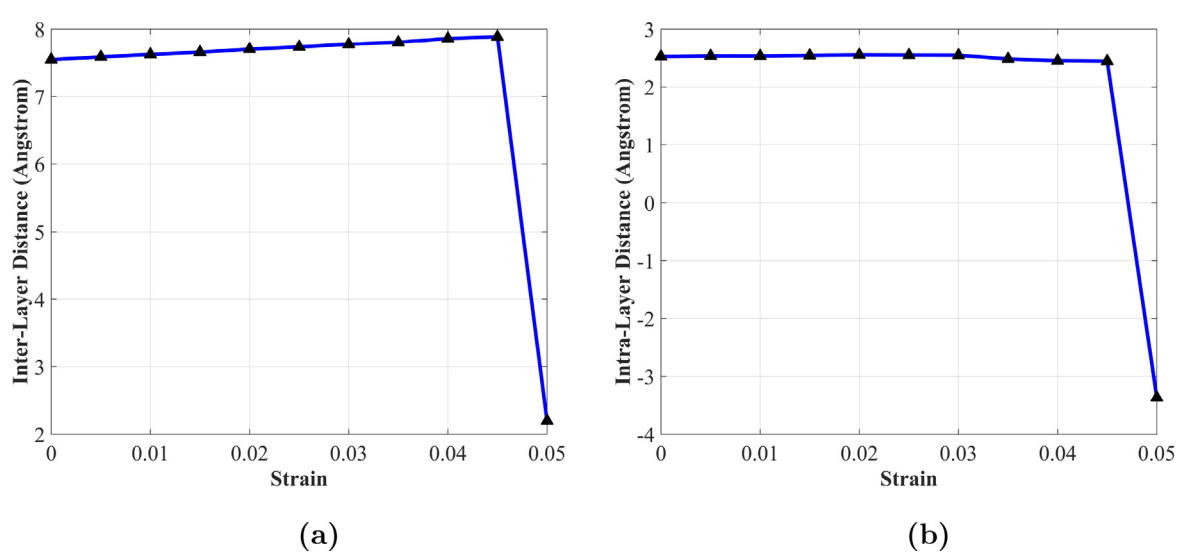

Fig. 6. (a) Evolution Inter-layer distance for triaxial tension and (b) Evolution Intra-layer distance for triaxial tension. (simulation conditions: pressure = 1 atm and temperature = 298 K).

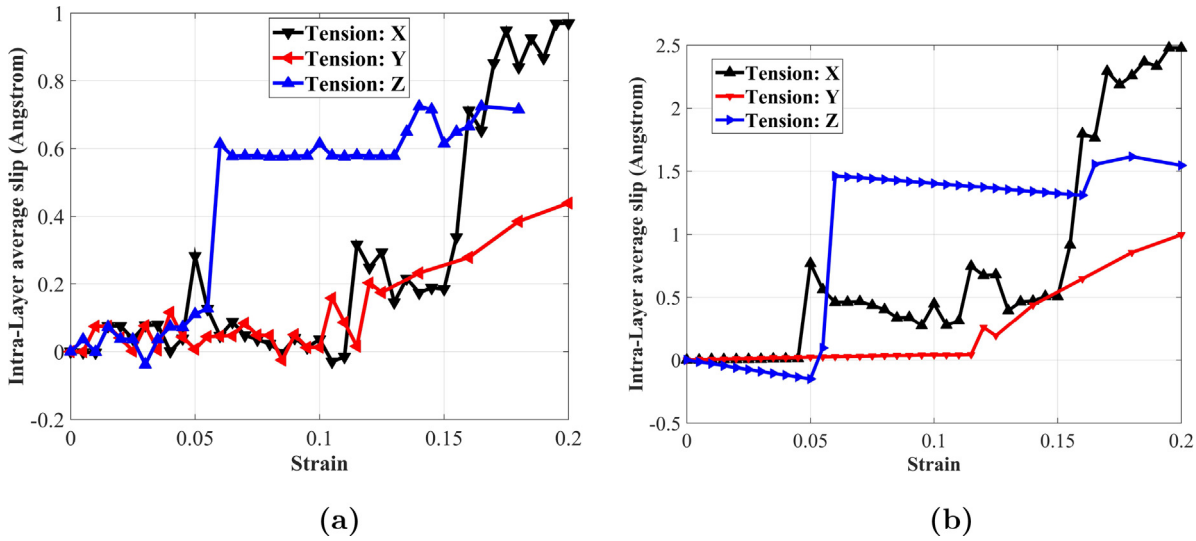

Fig. 7. (a) Evolution average layer slip in X direction and (b) Evolution average layer slip in Z direction. (simulation conditions: pressure = 1 atm and temperature = 298 K).

Fig. 1. It can be observed that for Y direction tensile loading, there is no slip observed in the stress–strain pre-peak regime as the layers are perpendicular to Y direction. However in the post-peak regime, layer slippage increases significantly. The layer slippage is demonstrated in the deformed simulation box (projected along the YZ plane) through Fig. 8. This graphical representations demonstrates that there is a sudden rearrangement of atoms from one particular order to that of another order thereby resulting increase in strain and reduction in stress (as seen in Fig. 2a for Y direction load) which is manifested as a slip type response(associated with increase in slip as demonstrated in Fig. 7a and b for Y direction loading). It should also be noted that as the slip increases, the increase in interlayer distance is reduced (since we observe a drop in Fig. 5a); moreover it could also be observed that intralayer distance decreases in contrast to the increase as observed before (refer Fig. 5b).

For loading along the X direction, a sharp increase in layer slip is observed at strain corresponding to the peak stress at around 0.05 (refer Fig. 2a). The corresponding deformed simulation box projected along XZ plane (refer Fig. 9) shows a sudden molecular rearrangement at the strain of 0.05. It should be noted that both the molecular arrangements are periodic in nature, even though the molecular arrangement of the two periodic structures is significantly different. This change in periodic structure of the molecular structure is also associated with a sudden increase in the average slip (ref Fig. 7a and b) at that strain level. Even though the slip almost remains constant in the Z direction but it reduces down to zero in the X direction. Thereafter at that changed molecular configuration (Ref. Fig. 9b) the layered structure takes in more loads leading to higher values of stress till a strain of 0.115 where again a sharp drop is observed in the stress–strain plots (Ref. Fig. 2a). An amorphization type of response is observed from the projected 2D XZ plane plots at that strain level explaining the reason for the sharp drop(Ref. Fig. 9c). With regards to the layer slip a sharp increase (ref Fig. 7a and b) changes could be observed with partial amorphization of the sample. The zig-zag nature of the curve indicates that the slip being observed is not in one specified direction but follows an oscillatory nature in the slip directions. Apart from sharp increase in layer slip (refer Fig. 7) a decrease could also be observed with that of the interlayer and the intralayer distances (refer Fig. 5). This suggests that with change in periodic orientation of the molecular structure, there is an increase in

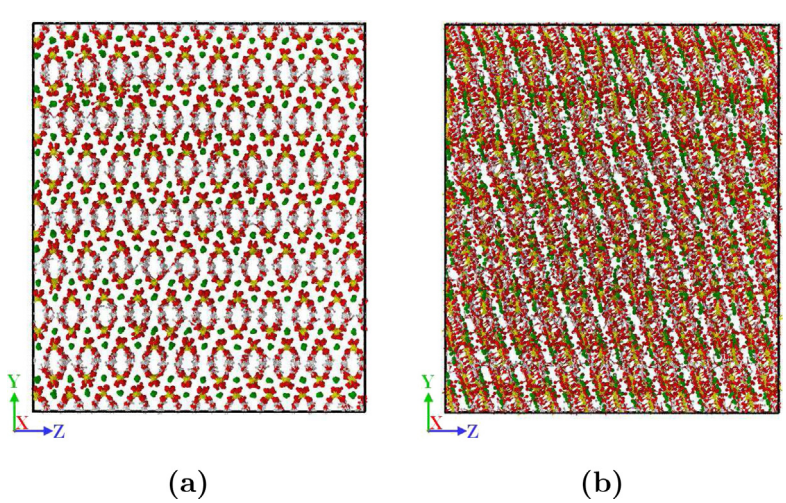

Fig. 8. Deformed simulation box projected on YZ plane under uniaxial stress along Y direction (Ca:green; S:yellow; H:white; O:red), (a) at strain level 0.115 (b) at strain level 0.12 (simulation conditions: pressure = 1 atm and temperature = 298 K). (For interpretation of the references to colour in this figure legend, the reader is referred to the web version of this article.)

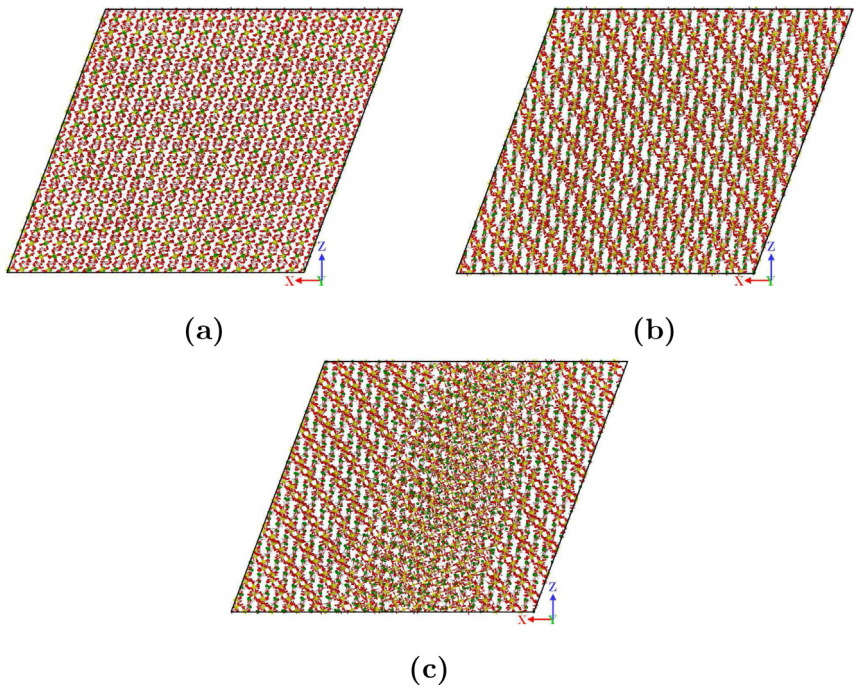

Fig. 9. Deformed simulation box projected on XZ plane under uniaxial stress along X direction (Ca:green; S:yellow; H:white; O:red), (a) at strain level 0.045 (b) at strain level 0.05 and (c) at strain level 0.115 (simulation conditions: pressure = 1 atm and temperature = 298 K). (For interpretation of the references to colour in this figure legend, the reader is referred to the web version of this article.)

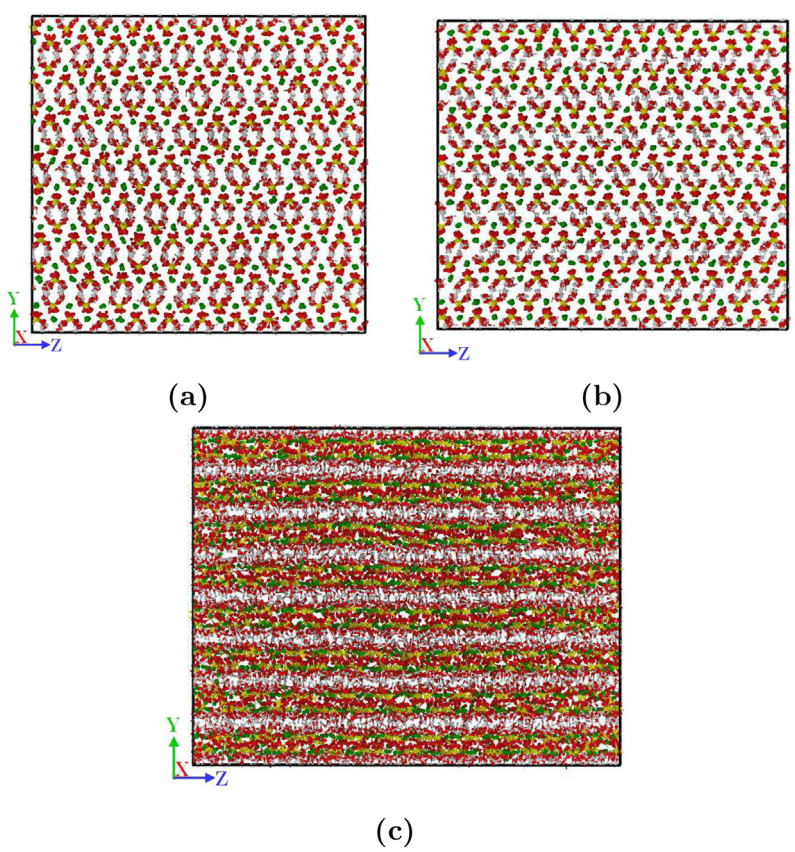

Fig. 10. Deformed simulation box projected on YZ plane under uniaxial stress along Z direction (Ca:green; S:yellow; H:white; O:red), (a) at strain level 0.055 (b) at strain level 0.06 and (c) at strain level 0.165 (simulation conditions: pressure = 1 atm and temperature = 298 K). (For interpretation of the references to colour in this figure legend, the reader is referred to the web version of this article.)

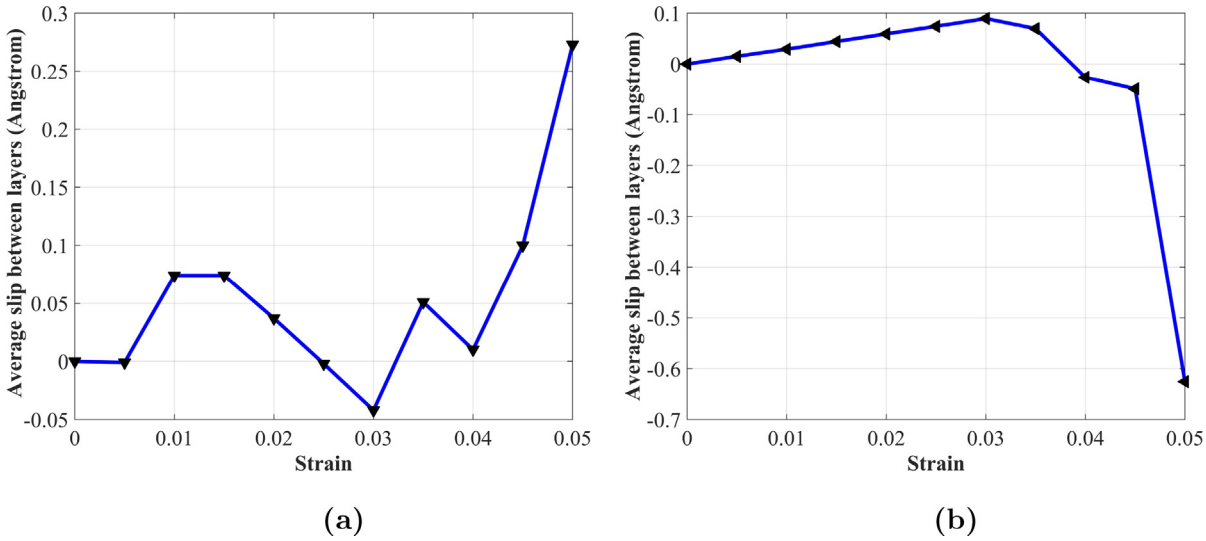

Fig. 11. (a) Evolution average layer slip in the direction of X for triaxial tension and (b) Evolution average layer slip in the direction of Z for triaxial tension. (simulation conditions: pressure = 1 atm and temperature = 298 K).

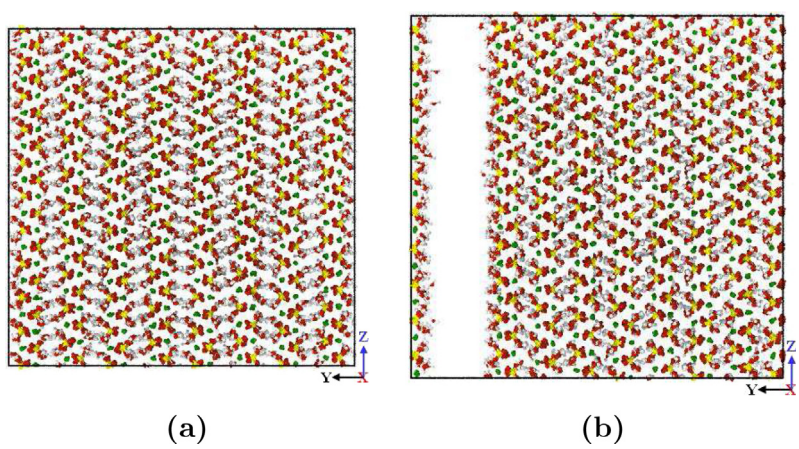

Fig. 12. Deformed simulation box projected on YZ plane under triaxial stress (Ca:green; S:yellow; H:white; O:red), (a) at strain level 0.045 and (b) at strain level 0.05. (simulation conditions: pressure = 1 atm and temperature = 298 K). (For interpretation of the references to colour in this figure legend, the reader is referred to the web version of this article.)

slip between the layers and also the interlayer and intralayer distances reduces significantly.

For uniaxial loading along the Z direction, the behavior of slip in the X direction is similar to that of the other two directions, but the slip value in the Z direction is observed to change even in the prepeak regime (quite contrary to the behavior observed in the other two directions) (refer Fig. 7). Graphical representation of the molecular rearrangement (YZ plane projection) can be observed from Fig. 10 when subjected to different strain levels in the prepeak and two post-peak regime. Similar to the X direction loading, one peak at around 0.06 strain (Fig. 2a) is associated with a change of one periodic structure of the molecule to that of another periodic structure (Ref. Fig. 10a and b). Associated with that change, similar behavior is observed in the interlayer and the intralayer distances (as that of the X direction) (refer Fig. 5a and b). However, it should be noted that as the structure becomes entirely amorphous, significant increase in intralayer is observed along with the interlayer (demonstrating differences in response with the X direction loading). For the slips in X and Z direction (refer Fig. 7a and b) we observe sharp increase at a strain level of 0.06 and constant behavior after that. As the amorphization takes place at higher strains (Fig. 10c) no significant changes in slip responses are observed. Above the strain level of 0.165 the structure is heading towards the amorphous state and no longer been able to sustain large stress.

Layer slippage mechanism has also been studied for triaxial loading case and has been demonstrated through Fig. 11. Prepeak slip value is almost steadily oscillating in X direction whereas it is steadily increasing up to a strain level of 0.03 for Z direction. Increment of the computed value around strain of 0.05 is attributed to sudden separation of layer caused by the brittle failure of the simulated sample as shown in Fig. 12.

4. Conclusion

Response of pristine single crystal gypsum subjected to tensile loading has been probed in this study at a molecular level. The suitability of the force potential used for molecular dynamic simulations has been validated through comparison with experimental investigations in its ability to predict elastic constants. The contribution of different energy contributing parts to the total energy of

the system subjected to loading has been investigated and it was found that the non-bonded part plays the major role both for triaxial and uniaxial stress type tensile loading situations. Detailed study has been carried out to investigate the contribution of the non-bonded part through estimation of intra-layer and inter-layer separation distance and average slip in between the layers. Significant differences in response were also observed for uniaxial and triaxial loading of the sample. The uniaxial response demonstrates a anisotropic behavior. The explanation of interlayer and interlayer separation response along with the slip response for the different types of tensile loading situations (as considered in this manuscript) has been given by observing the changes in molecular structure upon loading.

The characterization methodology developed in this study linking energy contribution with layer separation and layer slippage study is expected to pave the way for further molecular level studies of these types of materials with layered microstructure. Response behavior of these layered materials can be studied with this type of characterization framework under different types of loading situations.

Conflict of interest

The authors declared that there is no conflict of interest.

Acknowledgments

Authors acknowledge the support of computational facilities provided by Centre for Theoretical Studies, IIT Kharagpur.

References

[1] Iowa Geological Survey, F.A. Wilder, Gypsum: Its Occurrence, Origin, Technology and Uses. With Special Chapters Devoted to Gypsum in Iowa, Iowa, Geological Survey, 1918.
[2] NASA/JPL, 2018, Tiny crystal shapes get close look from mars rover, URL https://www.jpl.nasa.gov/news/news.php?feature=7057.
[3] E.A. Cloutis, M.A. Craig, J.F. Mustard, R.V. Kruzelecky, W.R. Jamroz, A. Scott, D.L. Bish, F. Poulet, J.-P. Bibring, P.L. King, Stability of hydrated minerals on mars, Geophys. Res. Lett. 34 (2007) L20202.
[4] N.-X. Geilfus, R. Galley, M. Cooper, N. Halden, A. Hare, F. Wang, D. Søgaard, S. Rysgaard, Gypsum crystals observed in experimental and natural sea ice, Geophys. Res. Lett. 40 (2013) 6362–6367.
[5] C. Meade, R. Jeanloz, Deep-focus earthquakes and recycling of water into the earth's mantle, Science 252 (5002) (1991) 68–72.
[6] H. Milsch, M. Priegnitz, Evolution of microstructure and elastic wave velocities in dehydrated gypsum samples, Geophys. Res. Lett. 39 (2012) L24305.
[7] S.-C. Ko, D.L. Olgaard, U. Briegel, The transition from weakening to strengthening in dehydrating gypsum: evolution of excess pore pressures, Geophys. Res. Lett. 22 (9) (1995) 1009–1012.
[8] E. Huang, J.-A. Xu, J.-F. Lin, J.-Z. Hu, Pressure-induced phase transitions in gypsum, Int. J. High Pressure Res. 17 (1) (2000) 57–75.
[9] L. Sarma, P. Prasad, N. Ravikumar, Raman spectroscopic study of phase transitions in natural gypsum, J. Raman Spectrosc. 29 (9) (1998) 851–856.
[10] P. Comodi, S. Nazzareni, P.F. Zanazzi, S. Speziale, High-pressure behavior of gypsum: a single-crystal X-ray study, Am. Mineral. 93 (10) (2008) 1530–1537.
[11] L. Gracia, A. Beltran, D. Errandonea, J. Andres, CaSO4 and its pressure-induced phase transitions. a density functional theory study, Inorg. Chem. 51 (3) (2011) 1751–1759.
[12] Y. Xin, S. Hou, L. Xiang, Y.-X. Yu, Adsorption and substitution effects of Mg on the growth of calcium sulfate hemihydrate: an ab initio dft study, Appl. Surf. Sci. 357 (2015) 1552–1557.
[13] Y. Xin, L. Xiang, Y.-X. Yu, Influence of structure on the morphology of CaSO4·n H_2O (n= 0, 0·5, 2): a molecular simulation study, Mater. Res. Innovations 19 (sup2) (2015) S2–103.
[14] H. Milsch, M. Priegnitz, G. Blöcher, Permeability of gypsum samples dehydrated in air, Geophys. Res. Lett. 38 (2011) L18304.
[15] H.F. Taylor, Cement Chemistry, Thomas Telford, 1997.
[16] A. Bentur, Effect of gypsum on the hydration and strength of C3S pastes, J. Am. Ceram. Soc. 59 (5–6) (1976) 210–213.
[17] F. Winnefeld, B. Lothenbach, Hydration of calcium sulfoaluminate cements–experimental findings and thermodynamic modelling, Cem. Concr. Res. 40 (8) (2010) 1239–1247.
[18] B.F. Pedersen, D. Semmingsen, Neutron diffraction refinement of the structure of gypsum, CaSO4.2H2O, Acta Crystallogr. Sect. B: Struct. Crystallogr. Crystal Chem. 38 (4) (1982) 1074–1077.
[19] C.D. Adam, Atomistic modelling of the hydration of CaSO4, J. Solid State Chem. 174 (1) (2003) 141–151.
[20] S. Haussühl, Elastische und thermoelastische eigenschaften von CaSO4·2H2O (gips), Zeitschrift für Kristallographie-Crystalline, Materials 122 (1–6) (1965) 311–314.
[21] H. Heinz, T.-J. Lin, R. Kishore Mishra, F.S. Emami, Thermodynamically consistent force fields for the assembly of inorganic, organic, and biological nanostructures: the interface force field, Langmuir 29 (6) (2013) 1754–1765.
[22] R.K. Mishra, A.K. Mohamed, D. Geissbhler, H. Manzano, T. Jamil, R. Shahsavari, A.G. Kalinichev, S. Galmarini, L. Tao, H. Heinz, R. Pellenq, A.C. van Duin, S.C. Parker, R.J. Flatt, P. Bowen, cemff: A force field database for cementitious materials including validations, applications and opportunities, Cem. Concr. Res. 102 (2017) 68–89.
[23] H. Heinz, H. Ramezani-Dakhel, Simulations of inorganic–bioorganic interfaces to discover new materials: insights, comparisons to experiment, challenges, and opportunities, Chem. Soc. Rev. 45 (2) (2016) 412–448.
[24] S. Rawat, N. Mitra, Compression twinning and structural phase transformation of single crystal titanium under uniaxial compressive strain conditions: comparison of inter-atomic potentials, Comput. Mater. Sci. 126 (2017) 228–237.
[25] S. Rawat, N. Mitra, Molecular dynamics investigation of c-axis deformation of single crystal Ti under uniaxial stress conditions: evolution of compression twinning and dislocations, Comput. Mater. Sci. 141 (2018) 19–29.
[26] S. Rawat, N. Mitra, Evolution of tension twinning in single crystal Ti under compressive uniaxial strain conditions, Comput. Mater. Sci. 141 (2018) 302–312.
[27] W. Heijnen, P. Hartman, Structural morphology of gypsum, brushite and pharmacolite, J. Cryst. Growth 108 (1991) 290–300.
[28] H. Sun, Force field for computation of conformational energies, structures, and vibrational frequencies of aromatic polyesters, J. Comput. Chem. 15 (7) (1994) 752–768.
[29] F. Module, Material studio 7.0, Accelrys Inc., San Diego, CA.
[30] D.N. Theodorou, U.W. Suter, Atomistic modeling of mechanical properties of polymeric glasses, Macromolecules 19 (1) (1986) 139–154.
[31] S. Plimpton, P. Crozier, A. Thompson, Lammps-large-scale atomic/molecular massively parallel simulator, Sandia National Laboratories 18.
[32] L. Tao, R. Shahsavari, Diffusive, displacive deformations and local phase transformation govern the mechanics of layered crystals: the case study of tobermorite, Scientific Reports 7 (1) (2017) 5907.
[33] N. Zhang, P. Carrez, R. Shahsavari, Screw-dislocation-induced strengthening–toughening mechanisms in complex layered materials: the case study of tobermorite, ACS Appl. Mater. Interfaces 9 (2) (2017) 1496–1506.
[34] N. Zhang, R. Shahsavari, Balancing strength and toughness of calcium-silicate-hydrate via random nanovoids and particle inclusions: atomistic modeling and statistical analysis, J. Mech. Phys. Solids 96 (2016) 204–222.
[35] R.W. Hockney, J.W. Eastwood, Computer Simulation using Particles, Crc Press, 1988.